



Cite this: *Nanoscale*, 2014, **6**, 14939

## New insights into the early stages of silica-controlled barium carbonate crystallisation†

Josef Eiblmeier,<sup>a</sup> Ulrich Schürmann,<sup>b</sup> Lorenz Kienle,<sup>b</sup> Denis Gebauer,<sup>c</sup> Werner Kunz<sup>a</sup> and Matthias Kellermeier<sup>\*d</sup>

Recent work has demonstrated that the dynamic interplay between silica and carbonate during co-precipitation can result in the self-assembly of unusual, highly complex crystal architectures with morphologies and textures resembling those typically displayed by biogenic minerals. These so-called biomorphs were shown to be composed of uniform elongated carbonate nanoparticles that are arranged according to a specific order over mesoscopic scales. In the present study, we have investigated the circumstances leading to the continuous formation and stabilisation of such well-defined nanometric building units in these inorganic systems. For this purpose, *in situ* potentiometric titration measurements were carried out in order to monitor and quantify the influence of silica on both the nucleation and early growth stages of barium carbonate crystallisation in alkaline media at constant pH. Complementarily, the nature and composition of particles occurring at different times in samples under various conditions were characterised *ex situ* by means of high-resolution electron microscopy and elemental analysis. The collected data clearly evidence that added silica affects carbonate crystallisation from the very beginning (*i.e.* already prior to, during, and shortly after nucleation), eventually arresting growth on the nanoscale by cementation of BaCO<sub>3</sub> particles within a siliceous matrix. Our findings thus shed light on the fundamental processes driving bottom-up self-organisation in silica-carbonate materials and, for the first time, provide direct experimental proof that silicate species are responsible for the miniaturisation of carbonate crystals during growth of biomorphs, hence confirming previously discussed theoretical models for their formation mechanism.

Received 17th September 2014,  
Accepted 8th October 2014

DOI: 10.1039/c4nr05436a

www.rsc.org/nanoscale

## Introduction

Modern approaches for the design of advanced materials with specific properties often follow bottom-up synthesis strategies starting from simple, molecular-scale components.<sup>1–4</sup> Based on this concept, it has for instance been possible to induce concerted self-assembly of inorganic minerals into elaborate, higher-order architectures using custom-designed polymers as

structure-directing agents.<sup>5–7</sup> Such studies are typically inspired by natural biomineralisation, where an organic matrix controls the crystallisation of inorganic matter to produce superior hybrid structures.<sup>8–13</sup> However, there are also other examples of complex mineralisation phenomena, which do not require organic species but may readily occur in purely inorganic environments. Among these, the processes observed during precipitation of alkaline-earth carbonates into alkaline, silica-containing media are probably the most prominent and well-studied case.<sup>14–31</sup> Under the influence of dissolved silicate as a crystallisation modifier, metal carbonates (usually BaCO<sub>3</sub>) can indeed assemble spontaneously into a range of sinuously shaped non-crystallographic aggregates (such as regular helioids), which mimic products from biomineralisation closely in terms of morphology and internal hierarchy, and therefore were termed “silica-carbonate biomorphs”.<sup>16,32,33</sup> The structural complexity of these peculiar materials relies on the fact that they are constituted of a multitude of uniform carbonate nanocrystals, which are largely co-oriented and thus generate mesoscopic order in the mature aggregates (as a third level of hierarchy in addition to molecular ordering on the nanometre-scale and morphological control on the micron-scale).<sup>17,24,27</sup>

<sup>a</sup>Institute of Physical and Theoretical Chemistry, University of Regensburg, Universitätsstrasse 31, D-93040 Regensburg, Germany. E-mail: werner.kunz@ur.de; Fax: (+49) 941 943 4532; Tel: (+49) 941 943 4044

<sup>b</sup>Technical Faculty, Synthesis and Real Structure, Christian-Albrechts-University Kiel, Kaiserstrasse 2, D-24143 Kiel, Germany. E-mail: lk@tf.uni-kiel.de; Fax: (+49) 431 880 6196; Tel: (+49) 431 880

<sup>c</sup>Physical Chemistry, University of Konstanz, Universitätsstrasse 10, D-78464 Konstanz, Germany. E-mail: denis.gebauer@uni-konstanz.com; Fax: (+49) 7531 88 3139; Tel: (+49) 7531 88 2169

<sup>d</sup>Material Physics, BASF SE, Carl-Bosch-Strasse 38, D-67056 Ludwigshafen, Germany. E-mail: matthias.kellermeier@basf.com; Fax: (+49) 621 66 43388; Tel: (+49) 621 60 43388

† Electronic supplementary information (ESI) available: Additional titration data (Fig. S1 and S2) and further results from TEM-EDX analyses (Fig. S3–S8). See DOI: 10.1039/c4nr05436a



After a recent surge of interest in this field,<sup>18–31</sup> it has been proposed that the formation of biomorphs is driven by an autocatalytic co-precipitation cycle, in which the components are alternately mineralised due to their opposite trends of solubility with pH.<sup>20,21,26</sup> In essence, it is assumed that growth of carbonate particles in alkaline solutions is accompanied by a reduction of the local pH (with respect to the bulk), due to reinforced dissociation of bicarbonate near active surfaces ( $\text{Ba}^{2+} + \text{HCO}_3^- \rightarrow \text{BaCO}_3 + \text{H}^+$ ). This pH gradient leads to enhanced protonation of silicate species in the vicinity of the carbonate particles, triggering condensation reactions and finally resulting in precipitation of a layer of amorphous silica around the nanocrystals soon after nucleation ( $\text{SiO}(\text{OH})_3^- + \text{H}^+ \rightarrow \text{Si}(\text{OH})_4 \rightarrow \text{SiO}_2 + 2\text{H}_2\text{O}$ ).<sup>20,21,26,27</sup> As polymerisation of silica proceeds at the surface, the local pH is in turn re-increased (due to continuous consumption of acidic silanol groups during condensation), thus raising the local carbonate supersaturation ( $\text{HCO}_3^- + \text{OH}^- \rightarrow \text{CO}_3^{2-} + \text{H}_2\text{O}$ ) and ultimately facilitating nucleation of novel  $\text{BaCO}_3$  crystallites, which by themselves will be cemented with silica in the following. This feedback loop is thought to ensure constant supply of the growing aggregates with nanometric building blocks, and hence represents the driving force for ordered polycrystalline mineralisation.<sup>20,21,26,27</sup>

In view of the model outlined above, one would expect that each of the nanorods constituting the final crystal aggregates is coated with an individual layer of silica. Indeed, such core-shell structures could be experimentally verified for hybrid nanoparticles of amorphous calcium carbonate (ACC)<sup>34</sup> or barium carbonate<sup>35</sup> and silica produced at high supersaturation. However, direct analyses of thin sections of mature biomorphs only confirmed the presence of small amounts of silica on the nanocrystals, whereas distinct outer layers could not be observed.<sup>24</sup> Consequently, the detailed role of the silica species in the stabilisation of  $\text{BaCO}_3$  nanoparticle units during growth of biomorphs has not yet been clarified. Therefore, we have used a titration-based technique in order to gain deeper insight into the pre- and early post-nucleation stages of barium carbonate crystallisation under the influence of dissolved silica, which we consider to be crucial steps in the progress of bottom-up self-assembly. In particular, we have performed precipitation assays in which the supersaturation of  $\text{BaCO}_3$  was gradually increased up to the point of nucleation and beyond, while the solution chemistry (and the effect of silica thereon) was continually monitored. Similar experiments have recently been employed to investigate the nucleation of calcium carbonate<sup>36–38</sup> and calcium phosphate<sup>39</sup> in general, as well as to study the impact of various soluble additives on  $\text{CaCO}_3$  crystallisation pathways.<sup>40–43</sup> In analogy with earlier work, precipitation was induced by slowly adding dilute barium chloride solution to an excess of sodium carbonate/bicarbonate buffer containing different amounts of dissolved silica, at concentrations and pH levels simulating the conditions where growth of silica biomorphs is typically observed.<sup>17,24–28,44,45</sup> During addition, the  $\text{Ba}^{2+}$  potential was recorded *in situ* with the aid of an ion-selective electrode,

while the pH was kept constant by back-titration with sodium hydroxide. Based on the measured values, actual concentrations of free and bound barium and carbonate ions were calculated, and used to compare time-dependent progressions obtained for different silica contents with reference scenarios traced in the absence of the additive. The resulting data are then combined with *ex situ* analyses of nucleated particles, carried out by means of high-resolution electron microscopy (HRTEM) and energy-dispersive X-ray (EDX) spectroscopy. Taken together, our findings paint a consistent picture of the effect of silica on the nucleation and growth of barium carbonate, which can be extrapolated to explain the role of the additive in the formation of biomorphs at the nanometre level.

## Experimental

### pH-constant titration measurements

Titration measurements were performed on a commercially available setup manufactured by Metrohm (Filderstadt, Germany). It consists of a Titrando 809 device that controls two attached Dosino 807 dosing units, capable of dispensing liquids at volume steps of down to 0.2  $\mu\text{L}$ . Experiments were carried out in an oil-jacketed vessel held at  $25.0 \pm 0.2$  °C, into which initially 50 mL of 5 mM carbonate buffer solution were given. Buffers were prepared by mixing appropriate volumes of 5 mM  $\text{Na}_2\text{CO}_3$  (Aldrich, anhydrous,  $\geq 99.8\%$ ) and 5 mM  $\text{NaHCO}_3$  (Riedel de-Haën,  $\geq 99.7\%$ ), in order to achieve final pH values of 10, 10.5 and 11, respectively (the latter being the pH of a neat 5 mM  $\text{Na}_2\text{CO}_3$  solution). The three distinct pH levels were chosen because the formation of biomorphs from solution has recently been reported to be most efficient in this range.<sup>28</sup> The concentration of the carbonate buffers used for crystallisation had to be reduced from 10 to 5 mM as compared to previous studies on calcium carbonate,<sup>36–38</sup> as it turned out that barium carbonate precipitated preferentially at the outlet of the  $\text{BaCl}_2$  solution in 10 mM  $\text{Na}_2\text{CO}_3$ - $\text{NaHCO}_3$  at all studied pH values. Silica was introduced by dissolving 5 mM  $\text{Na}_2\text{CO}_3$  in different dilutions of commercial water glass (concentrated sodium silicate solution, Aldrich, reagent grade), leading to the final  $\text{SiO}_2$  concentrations of 300, 600, and 1200 ppm (500–600 ppm being the usual silica content of mother solutions in a typical synthesis of biomorphs<sup>17,24–28,44,45</sup>). The pH of the silica-carbonate mixtures was subsequently adjusted to the particular target value using aliquots of either 1 M NaOH or 1 M HCl (both Merck, p.a.), whereby the concomitant dilution was negligible.

In the actual measurements, 10 mM barium chloride solution (prepared from  $\text{BaCl}_2 \cdot 2\text{H}_2\text{O}$ , Riedel de-Haën,  $\geq 99\%$ ) was continuously added to the buffer at a rate of 0.01 mL  $\text{min}^{-1}$  (with or without silica and at different pH levels). The pH of the buffer was kept constant at its set value by automatic counter-titration with 10 mM sodium hydroxide (Riedel-de Haën, standard solution). During titration, the  $\text{Ba}^{2+}$  potential and the pH of the sample were monitored online by means of an ion-selective electrode (ISE; Mettler-Toledo, DX337-Ba) and



a flat-membrane glass electrode (Metrohm, no. 6.0508.110), which simultaneously served as the reference for the  $\text{Ba}^{2+}$ -selective half-cell. Calibration of the ISE was achieved by titrating  $\text{BaCl}_2$  into water (brought to the same pH as the respective buffer by NaOH addition) and measuring the  $\text{Ba}^{2+}$  potential as a function of the known solution concentration, using identical settings as in the precipitation assay. The glass electrode was calibrated weekly with buffers of pH 4.0, 7.0 and 9.0 (purchased from Metrohm). After every experiment, the beaker, burette tips and electrodes were washed with acetic acid (10%) to remove crystallised carbonate, and subsequently rinsed with water.

The recorded  $\text{Ba}^{2+}$  potentials were first corrected for the interfering influence of sodium ions (using the Nikolsky–Eisenman equation<sup>46</sup> and the electrode selectivity coefficient for  $\text{Na}^+$  given by the manufacturer,  $\log K_{\text{Na}} = -0.9$ ), and then translated into apparent free concentrations *via* the calibration data obtained in water. Since the volumes added to the reaction vessel are known at all times, free and bound amounts of barium ions can readily be computed from these concentrations and used to derive the corresponding values for the carbonate species in the system. This treatment assumes that  $\text{Ba}^{2+}$  and  $\text{CO}_3^{2-}$  ions bind in equimolar amounts (*i.e.* neutral associated species) and that the investigated dilute solutions behave like ideal systems; both of these assumptions have been verified explicitly for  $\text{CaCO}_3$  in recent studies.<sup>37,38,47</sup> Based thereon, time-dependent profiles for the free ion concentration products ( $\text{IP} = [\text{Ba}^{2+}]_{\text{free}} \cdot [\text{CO}_3^{2-}]_{\text{free}}$ ) were calculated and are discussed in the following.

### TEM and EDX analyses

Precipitates formed in the titration experiments were isolated at distinct times by filtering the samples through 200 nm membranes (Whatman, mixed cellulose esters) and washing the remaining particles with ethanol (Baker, p.a.). The dried powder was then re-dispersed in ethanol, and aliquots of the resulting suspension were placed on carbon-film copper grids (Plano GmbH, 200 mesh). The excess liquid was carefully removed with a small piece of filter paper, before allowing the remaining precipitates to dry in air. The as-obtained particles were investigated routinely with a Philips CM 12 microscope at an acceleration voltage of 120 kV. Images were obtained using a Gatan TV 673 wide-angle camera and a TVIPS slow scan camera with external control utilising the EM-MENU 4 software. Selected specimens were further analysed at high resolution with a FEI Tecnai F30 STwin electron microscope (300 kV, field-emission gun, spherical aberration constant  $C_s = 1.2$  mm). STEM Z-contrast images were obtained with a HAADF detector. In order to reveal the composition of the particles, elemental mapping was performed on selected areas by means of an EDX system (Si/Li detector) mounted on the microscope.

For EDX analysis of powder samples, the filtered and dried particles were directly transferred onto conducting double-sided adhesive carbon tapes that were fixed on standard aluminum stubs. Samples were studied using a Hitachi TM3000 tabletop SEM operated at an acceleration voltage of 15 kV and

a working distance of 10 mm. EDX measurements were performed with the aid of an installed Bruker Quantax 70 detector. Spectra were recorded from not less than three different positions on the stub, and results were averaged for a given specimen.

## Results

### *In situ* potentiometric titrations

Fig. 1 shows the temporal evolution of the free ion products detected upon titration of barium chloride into carbonate

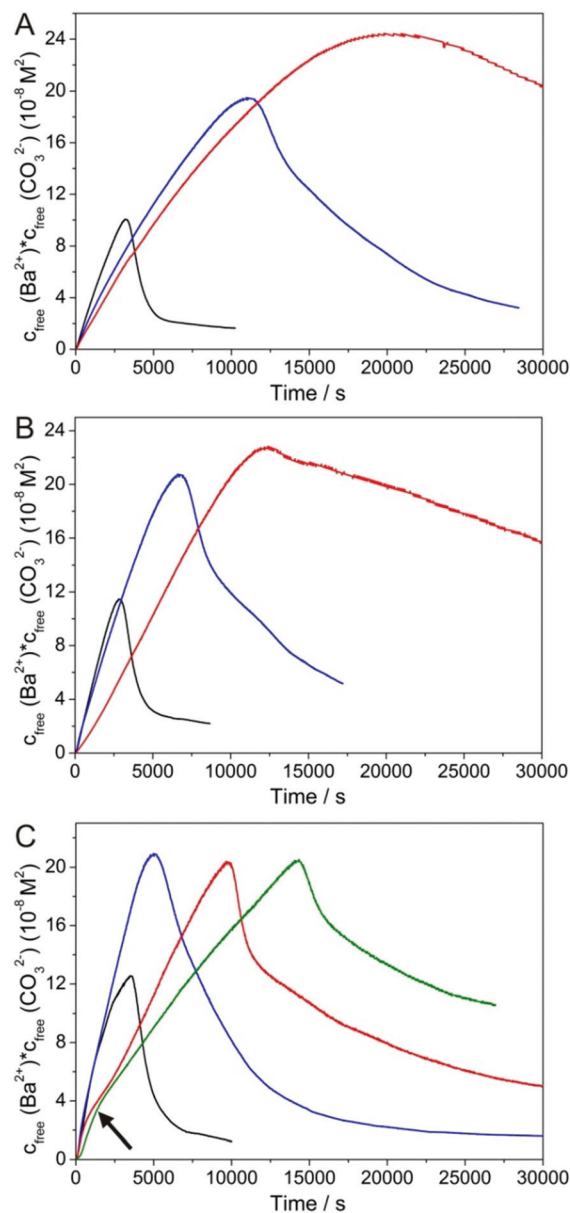


**Fig. 1** Time-dependent profiles for the free  $\text{BaCO}_3$  ion products traced during continuous addition of 10 mM  $\text{BaCl}_2$  to 5 mM  $\text{Na}_2\text{CO}_3$ – $\text{NaHCO}_3$  buffers at (A) pH 10, (B) pH 10.5, and (C) pH 11. Experiments were performed in the absence of silica (black curves) and in the presence of 300 ppm (blue curves), 600 ppm (red curves) and 1200 ppm  $\text{SiO}_2$  (green curve, only measured for pH 11).



buffers at different pH and silica contents. Regarding at first the reference experiments with no added silica (black curves), it is evident that the free ion product increases more or less linearly with time, until a critical point is reached and nucleation of  $\text{BaCO}_3$  occurs (maximum of the curve). Subsequently, the concentration of free  $\text{Ba}^{2+}$  and  $\text{CO}_3^{2-}$  ions in solution drops sharply and then gradually approaches a constant level that corresponds to the solubility of the initially precipitated phase. Comparison of measured solubilities ( $\text{IP} \approx 1\text{--}2 \times 10^{-8} \text{ M}^2$ , independent of pH) with the literature values for crystalline witherite ( $K_{\text{sp}}(\text{BaCO}_3) = 5 \times 10^{-9} \text{ M}^2$ )<sup>48</sup> suggests that under the given conditions, barium carbonate nucleates in an amorphous state, which exhibits a solubility similar to that of ACC nanoparticles produced in analogous experiments with calcium carbonate,<sup>36–38</sup> and soon transforms into a crystalline phase when left in contact with the mother solution (as shown more explicitly below). Alternatively, one may speculate that the higher solubility observed in the titrations reflects differences in the thermodynamic stability between bulk and nano-sized witherite, as reported previously for other minerals.<sup>49–51</sup>

Apart from that, we find that the amount of free  $\text{Ba}^{2+}$  detected in solution prior to nucleation is significantly lower than the dosed amount (see Fig. S1 in the ESI†), indicating the formation of  $\text{BaCO}_3$  ion pairs and/or larger clusters as in the case of calcium carbonate.<sup>36–38,52</sup> In fact, about 32, 52 and 65% of the added cations are bound in the prenucleation regime at pH 10, 10.5 and 11, respectively. Thus, the fraction of  $\text{Ba}^{2+}$  residing in ion associates is smaller than what has been observed for  $\text{Ca}^{2+}$  under similar conditions (about 75% bound at pH 10),<sup>36</sup> suggesting that  $\text{BaCO}_3$  ion pairs/clusters are somewhat less stable than their  $\text{CaCO}_3$  counterparts. Finally, it is worth mentioning that the time of nucleation does not vary significantly with pH (3140, 2810 and 3470 s at pH 10, 10.5 and 11, respectively), while the critical supersaturation required for nucleation to occur increases slightly as the pH is raised ( $\text{IP} \approx 1.00 \times 10^{-7}$ ,  $1.15 \times 10^{-7}$  and  $1.26 \times 10^{-7} \text{ M}^2$  at the point of nucleation at pH 10, 10.5 and 11, respectively). This, as well as the larger fraction of bound  $\text{Ba}^{2+}$  at higher pH, can be ascribed to changes in the carbonate/bicarbonate buffer equilibrium with pH (~30%  $\text{CO}_3^{2-}$  co-existing with  $\text{HCO}_3^-$  in solution at pH 10 vs. ~80% at pH 11).

The effect of silica as an additive in  $\text{BaCO}_3$  precipitation can now be evaluated by comparing titration profiles obtained in its presence with those seen in the reference experiments. In line with earlier work on calcium carbonate,<sup>40–43</sup> we discuss three distinct aspects in the curves: (i) the slope of the temporal increase in free  $\text{Ba}^{2+}$  prior to nucleation (reflecting the stability of ion associates in solution), (ii) the time of nucleation and any occurring delay of nucleation, and (iii) the level of the free ion product after nucleation (indicating the solubility/stability of the precipitated phase as well as possible interactions with formed particles, *e.g.* growth inhibition). Changes in these three parameters relative to the reference scenario are outlined as a function of pH and silica concentration in Fig. 2. Looking first at the prenucleation slopes (Fig. 2A, values determined by linear fits to experimental  $n_{\text{free}}(\text{Ba}^{2+})$ -time data, *cf.*

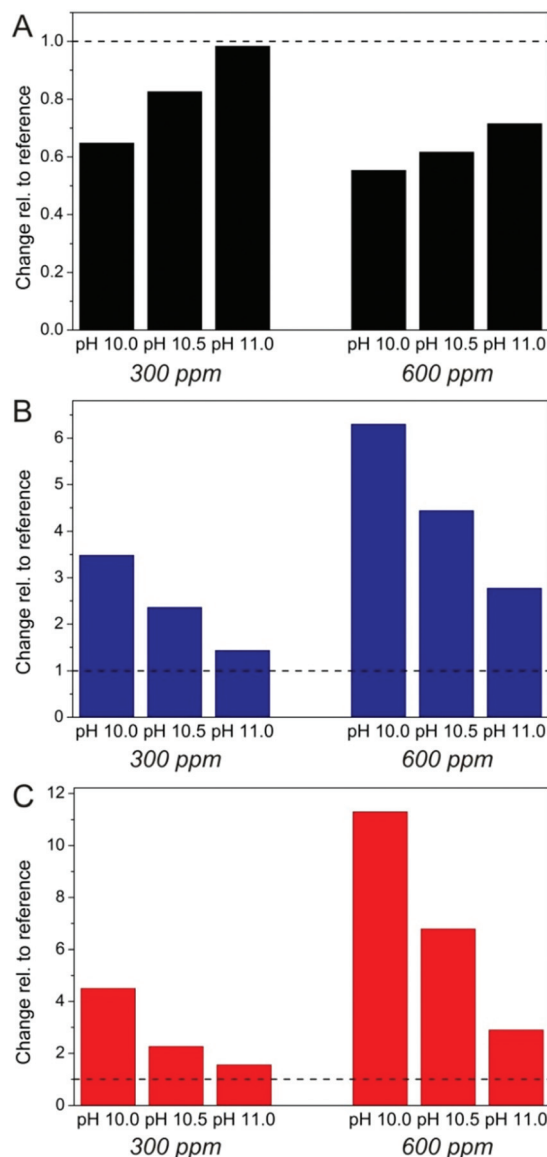


**Fig. 2** Bar plots illustrating the effect of added silica on (A) the slope of the titration curves in the prenucleation stage, (B) the nucleation time, and (C) the solubility of the initially precipitated phase for different pH levels and analytical silica concentrations (as indicated). Results are given as relative changes to the silicate-free reference experiments (as indicated), that is, as quotients of the respective values determined in the presence and in the absence of silica.

Fig. S1 in the ESI†), one can observe that addition of silica leads to a flattening of the curves, the extent of which depends on both the pH and the  $\text{SiO}_2$  content. Generally, flat slopes mean an enhanced binding tendency for the barium ions, which in the present case can be caused by two distinct effects. First, the cations could form complexes with the silicate species in the system. To assess such interactions independently of the influence of carbonate ions, we have performed a series of reference experiments where barium chloride was titrated into carbonate-free silica solutions under the same pH and concentration conditions. The results (see



Fig. S2 in the ESI†) show that there is no detectable binding of  $\text{Ba}^{2+}$  in the absence of carbonate at pH 10 for 300 and 600 ppm  $\text{SiO}_2$ , while at pH 10.5 about 20–30% of the added cations appear to be bound by silica at both concentrations. At pH 11, we could not again trace any significant complexation up to silicate contents of 600 ppm, whereas a reduction in free  $\text{Ba}^{2+}$  of around 30% was observed at 1200 ppm. This behaviour can be understood on the basis of pH-dependent changes in the speciation of silica in solution:<sup>53–55</sup> as the pH is decreased, enhanced condensation of siliceous species leads to a higher fraction of larger oligomers, which *per se* seem to be more suitable for the complexation of divalent cations. In turn, the number of charges at these oligomers – which obviously are essential for interaction with the cations – decreases at lower pH and therefore, strongest binding is found at an intermediate pH level, here about 10.5. Thus, complexation by silicate species may account to some extent for the observed flattening of the prenucleation slopes in carbonate buffers at pH 10.5 (and 11), but it cannot explain the trends seen in Fig. 2A, where changes clearly become more pronounced with decreasing pH and increasing silica concentration: at pH 10 and 600 ppm  $\text{SiO}_2$ , the slope is reduced to about 55% of the reference without silica, whereas there is hardly any effect at pH 11 and 300 ppm.

The second possible role of added silica in the prenucleation regime is to interact with associated species (that is,  $\text{BaCO}_3$  ion pairs and/or clusters) and stabilise them relative to the reference case, as also reported for a number of other soluble additives in previous studies on  $\text{CaCO}_3$ .<sup>40–43</sup> Again, one can envision that the silicate oligomers and polymers present at lower pH are more efficient in such stabilisation phenomena than the mono- and dimers prevailing at high pH. On the other hand, charge is not necessarily an important factor in this type of interaction, because ion pairs and clusters are supposed to be neutral solute entities. This would rationalise the observed trends and suggests that stabilisation of prenucleation species is the dominant effect of silica under the given conditions, while simple ion complexation only has a minor influence (also note that binding of barium ions by carbonate is significantly stronger than with silicate, as evidenced in Fig. S2 in the ESI†). Finally, it is worth mentioning that the curves recorded for 600 and 1200 ppm  $\text{SiO}_2$  at pH 11 follow the reference in the beginning, before they bend down after about 1000–2000 s (see the arrow in Fig. 1C) to subsequently increase at a smaller slope. This might hint at the formation of larger silicate oligomers during an initial induction period (likely due to  $\text{Ba}^{2+}$ -induced silica condensation),<sup>56</sup> which then – above some critical concentration – influence  $\text{BaCO}_3$  ion pairs and clusters in a way related to what is found for lower pH values.

Similar trends can be distinguished concerning the nucleation time (Fig. 2B). Here, it is evident that the presence of silica causes a noticeable delay of nucleation, and that the degree of retardation again depends on both the pH and the silica concentration. The corresponding inhibition factors (IF, defined as the ratio of the nucleation time in the presence of

silica to that in the additive-free reference experiment) demonstrate that the influence of silica becomes much more distinct at higher concentrations (IF = 3.5 and 6.3, respectively, for 300 and 600 ppm at pH 10). On the other hand, for a given silica content, the data show a clear and consistent decrease in the inhibition ability with increasing pH so that, at 300 ppm  $\text{SiO}_2$  and pH 11, there is merely a minor extent of retardation discernible (IF = 1.4). Consequently, oligomeric silicates seem to be much more suitable for impeding nucleation than monomers and dimers, in analogy with what has been observed with regard to the stabilisation of prenucleation species (Fig. 2A).

Nevertheless, the most drastic impact of silica on the early stages of  $\text{BaCO}_3$  crystallisation can be seen in the apparent solubility of the initially precipitated phase (Fig. 2C), which is higher in all silica-containing samples than in the references without silica. In fact, the free ion product measured at the end of the experiment at pH 10 and 600 ppm  $\text{SiO}_2$  exceeds that of the corresponding reference by a factor of more than 10. Another striking aspect of the precipitation behaviour in the presence of silica is that the level of free ions in solution does not fall to a constant solubility within the duration of the measurements (see Fig. 1). Rather, the free ion product decreases continuously and at a rate that is markedly slower than in the reference experiment. In some cases (300 ppm  $\text{SiO}_2$  at pH 10 and 10.5, and 600/1200 ppm at pH 11), we observed an initially steep decline which, at a more or less pronounced breakpoint, turns into a much flatter decay in the following. These findings suggest that the precipitated phase is not in equilibrium with the surrounding solution, so that its actual solubility product cannot be established (at least not during the studied period, except for the sample at pH 11 and 300 ppm  $\text{SiO}_2$ ). In other words, the nucleated particles cannot grow freely, likely because added silica inhibits also growth of  $\text{BaCO}_3$  (as will be further discussed below). Again, the effects become dramatically stronger when the concentration of silica is increased and/or the pH of the buffer is decreased (*cf.* Fig. 2C), indicating that growth inhibition is likewise performed in a more effective manner by oligomeric silicate species, which are more abundant at lower pH.

### Characterisation of nucleated particles

The precipitates formed at the end of each titration experiment were further analysed by means of transmission electron microscopy (Fig. 3). In the absence of silica (Fig. 3A–C), crystals with rod- or needle-like shapes and sizes in the micron-range (typically about 5  $\mu\text{m}$  in length and 1  $\mu\text{m}$  in width) were obtained, with no distinct variations being discernible between the samples produced at different pH values. Electron diffraction patterns confirmed these particles as well as those generated under the influence of silica to be orthorhombic, witherite-type barium carbonate (see Fig. S3–S5 in the ESI†). Addition of silica proved to have a drastic size-reducing effect on the resulting crystals, which thus became scaled down to dimensions in the nanometre regime (with characteristic lengths of 200–700 nm and widths of 1–50 nm, *cf.* Fig. 3D, E,



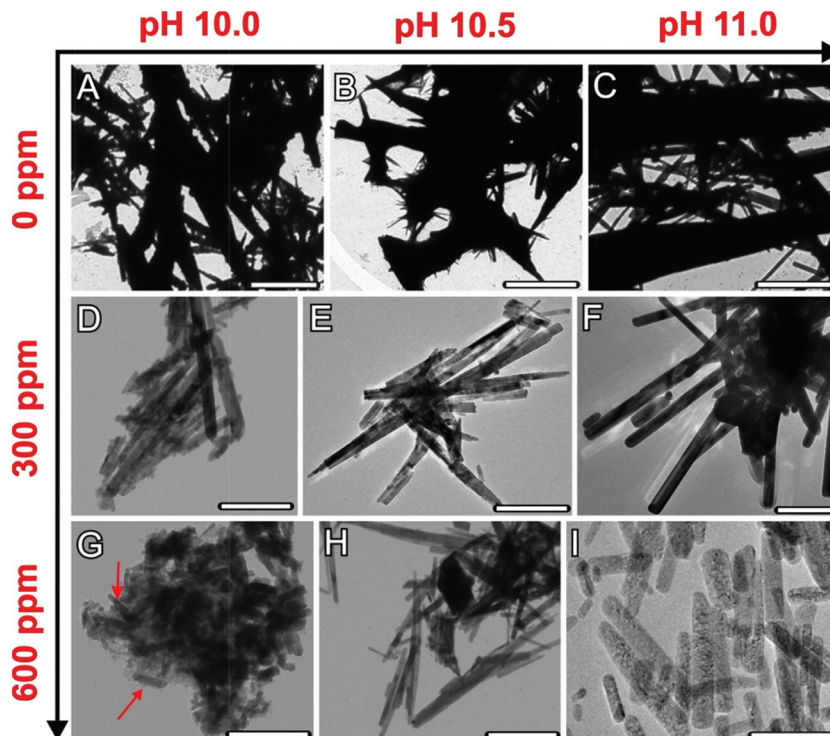


**Fig. 3** TEM images of crystals isolated at the end of titration experiments carried out at pH 10 (A, D, G), pH 10.5 (B, E, H), and pH 11 (C, F, I), in the presence of 0 (A–C), 300 (D–F), and 600 ppm silica (G–I). Note that addition of silica leads to a progressive miniaturisation of the formed carbonate crystals, from bulky micron-sized needles in the reference samples (A–C) to quite well-defined nanoparticles (highlighted by arrows in (G)) embedded in a matrix of amorphous silica at pH 10 and 600 ppm  $\text{SiO}_2$ . Scale bars are 3  $\mu\text{m}$  (A–C and F), and 300 nm (D, E and G–I).

and G–I). This is true for all silica-containing samples except for 300 ppm  $\text{SiO}_2$  at pH 11, where micron-sized crystals only slightly smaller than in the reference case were produced (Fig. 3F). These observations comply well with the results of the titration measurements, in which silica also showed only a minor influence on the precipitation behaviour under these conditions (*cf.* Fig. 1 and 2). Beyond that, we can also distinguish trends in the size of the nanoparticles that are consistent with (though not as clear as) those reflected in the titrations, that is the crystals become smaller as the silica content is raised or the pH is lowered. This is most evident in the sample at pH 10 and 600 ppm  $\text{SiO}_2$ , where fairly uniform nanorods, about 100 nm long and 20 nm wide and embedded in a matrix of silica, were generated (Fig. 3G).

In a further series of experiments, the composition of the precipitates formed under the distinct conditions was investigated by scanning EDX analysis and the HAADF-STEM mode (Fig. 4; see also Fig. S6 and S7 in the ESI†). Elemental maps of crystals grown at different silica contents demonstrate the presence of a continuous matrix of silica (visible as increased Si counts) around individual  $\text{BaCO}_3$  nanorods. The amount of silica associated with the carbonate crystals was determined independently by EDX spectroscopy of bulk powder samples (see Fig. S8 in the ESI†). It was found that the overall Si content in the precipitates depends on the silica concentration

in solution as well as on the pH of the buffer, with general tendencies that, again, very well match with those identified in the titrations. While the highest silica content is obtained at 600 ppm  $\text{SiO}_2$  and pH 10 ( $\text{Si}/\text{Ba} \approx 0.13$ ), lower amounts are detected when the pH is increased ( $\text{Si}/\text{Ba} \approx 0.09$  for 600 ppm at pH 10.5 and 11) or when less silica is added to the mother solution ( $\text{Si}/\text{Ba} \approx 0.08$  for 300 ppm at pH 10). Remarkably, we could not detect any significant counts for Si in the crystals formed at 300 ppm and pH 11, *i.e.* exactly under those conditions where no considerable downsizing was observed either (Fig. 3F). This suggests strongly that the silica content of the crystals and their size are interrelated, with higher Si levels being linked to smaller particles. On that basis, we can conclude that addition of silica provokes miniaturisation of  $\text{BaCO}_3$  particles formed during precipitation from solution.

To gain additional insight into the actual nucleation process of barium carbonate in the presence of silica, we have studied further samples that were drawn directly after the maximum in the titration curve ( $\sim 10\,500$  s for the system at pH 10.5 and 600 ppm  $\text{SiO}_2$ ). HRTEM micrographs of such specimens reveal a continuous solid matrix with relatively low electron contrast, which hosts numerous individual spots that exhibit higher contrast and measure only a few nanometres (3–5 nm) in diameter (Fig. 5). Interestingly, these nanoclusters grow in size (to about 10 nm) and become crystal-



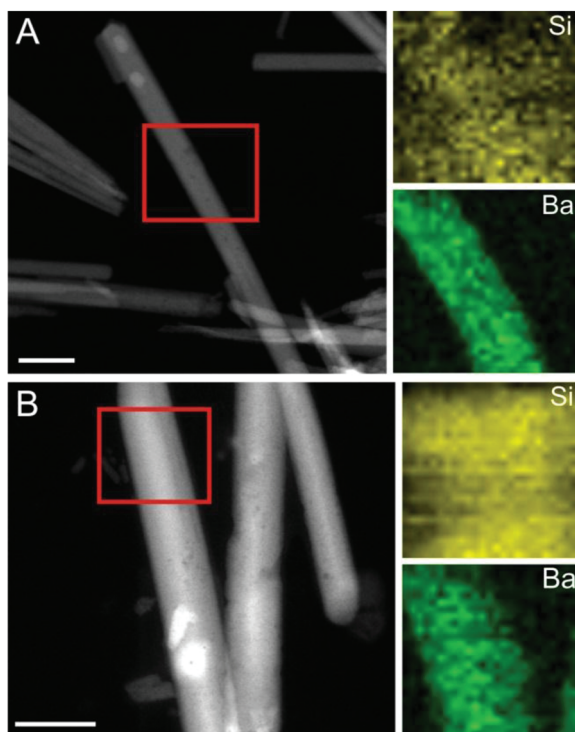


**Fig. 4** STEM images and the corresponding Si and Ba elemental maps for  $\text{BaCO}_3$  nanorods formed during titration of  $\text{BaCl}_2$  into carbonate buffer at pH 10, containing (A) 300 and (B) 600 ppm silica. The red rectangle marks the region analysed by EDX. The data show that increased counts of silicon are detected around the carbonate particles. Scale bars are 100 nm.

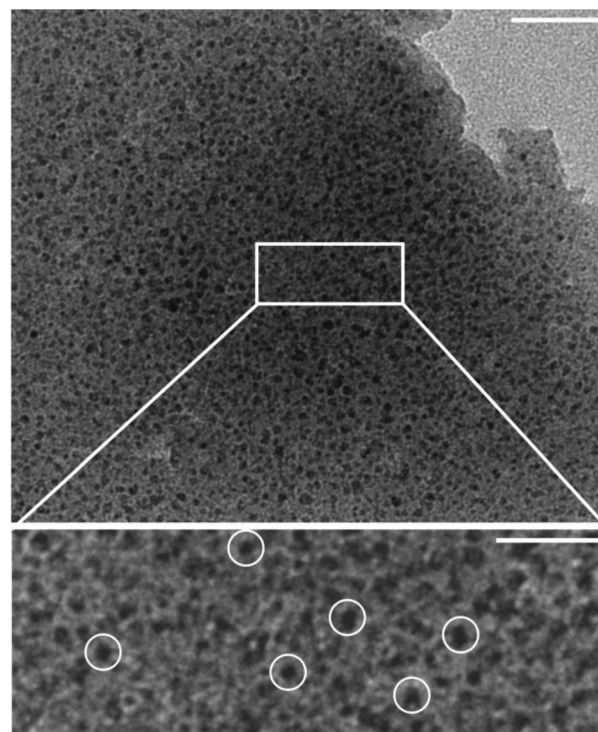


**Fig. 5** TEM images of  $\text{BaCO}_3$  nanoclusters (black spots) that are distributed throughout a matrix of lower electron contrast, presumably consisting of amorphous silica. These structures were isolated immediately after the maximum in free  $\text{Ba}^{2+}$  concentration had been reached in titrations at pH 10.5 and 600 ppm  $\text{SiO}_2$ . Scale bars are 40 nm (overview) and 20 nm (zoom).

line (with signatures typical for witherite) when exposed to the electron beam (Fig. 6A).

These are strong indications that the small units are  $\text{BaCO}_3$  clusters dispersed in a matrix of amorphous silica. In this regard, one may speculate that nucleation of  $\text{BaCO}_3$  proceeds *via* these clusters and involves their aggregation and final coalescence, as reported in detail for calcium carbonate.<sup>36,52,58</sup> The role of the silica would thus be to keep the clusters apart and hinder their agglomeration,<sup>43,59,60</sup> thereby delaying nucleation under otherwise identical conditions (as observed in the titrations). Growth of witherite crystals (and/or any possible amorphous precursors) might moreover occur through attachment (or fusion) of these primary units. This notion is supported by HRTEM images of mature crystals, in which domains with contours reminiscent of the spherical precursor particles can still be discerned (Fig. 6B).

## Discussion

In this work, we have used a titration-based setup to gain detailed insight into the nucleation of barium carbonate under the influence of dissolved silica at a constant pH, and correlated the obtained results with particle sizes and compositions determined for crystals isolated at the end of the exper-

iments. From the  $\text{Ba}^{2+}$  potentials monitored *in situ* during titration, it was possible to assess the multiple effects of added silica on distinct stages of nucleation and early growth in a quantitative manner, *i.e.* changes in the equilibria of ion associates existing in solution before nucleation, the ability of the additive to retard nucleation, and also its impact on the solubility (and thus nature) of the initially formed solid phase. All these parameters were noticeably affected in the presence of dissolved  $\text{SiO}_2$ , to an extent that depended on both the silica concentration and the pH of the system.

Concerning the prenucleation regime, our data show that  $\text{Ba}^{2+}$  and  $\text{CO}_3^{2-}$  ions undergo association into ion pairs and/or larger clusters as reported previously for  $\text{CaCO}_3$ ,<sup>36,47,52,58</sup> and that added silica is obviously capable of stabilising these species. The degree of stabilisation appears to be a function of the chemistry of silica in solution (apart from the additive concentration alone), with higher oligomers (as prevailing at lower pH) being more efficient than simple monomers or dimers. Although we can only speculate about possible reasons for this behaviour, it may be argued that oligomeric silicates encapsulate ion pairs or clusters and thereby effectively remove them from the equilibrium with the free ions, hence increasing the fraction of bound ions and rationalising the observed trends with pH.

In any case, this stabilising effect is accompanied by a delay of nucleation relative to the reference without added silica. In



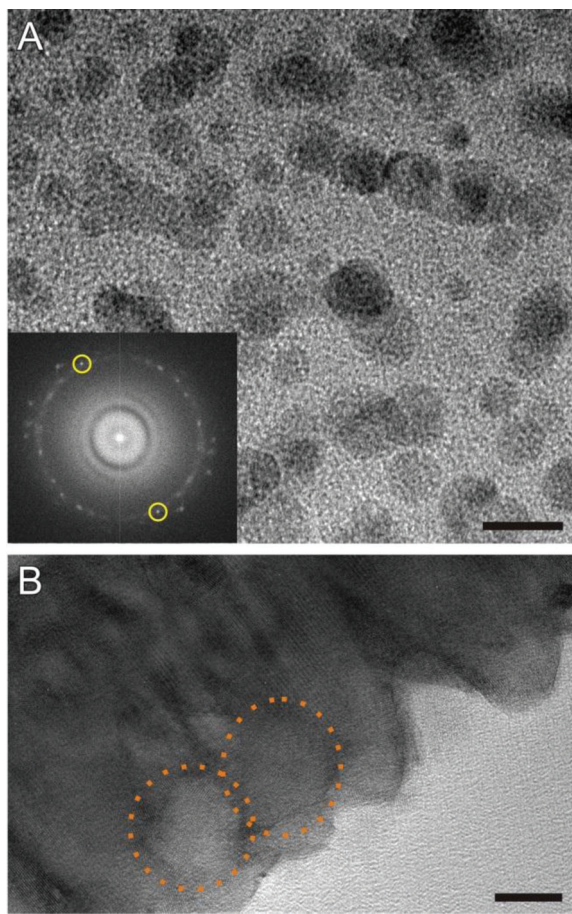


**Fig. 6** (A) TEM micrograph of  $\text{BaCO}_3$  nanoclusters which, upon prolonged exposure to the electron beam, grow to particles of ca. 10 nm in size (pH 10.5, 600 ppm  $\text{SiO}_2$ ). Inset: Fourier transform of the TEM image, showing distinct intense spots along a more or less continuous diffuse ring of intensity. The measured distance in-between the reflection pair marked in yellow corresponds to a lattice spacing of 2.1 Å which, within the common limits of error in electron diffraction, can be indexed to the (221) planes of witherite.<sup>57</sup> Scale bar: 10 nm. (B) HRTEM micrograph of a mature  $\text{BaCO}_3$  rod obtained from a sample at pH 11.0 and 600 ppm  $\text{SiO}_2$ . Close examination suggests that the crystal was formed *via* fusion of spherical primary particles, the contour of which can still be distinguished (highlighted by dotted orange circles). Scale bar: 10 nm.

light of the TEM analyses performed on precipitates isolated shortly after nucleation (Fig. 5 and 6), it seems that embedding of small clusters in a siliceous matrix is the basis for this inhibition. Again, lower pH and/or higher silica contents lead to stronger effects, suggesting that the ability of silica to condense and polymerise under the given conditions plays an important role in this context. Similar observations were recently made for mixtures of calcium carbonate and silica, where it was proposed that silicate species bind onto the periphery of ion clusters and thus generate a negative charge around them that causes mutual electrostatic repulsion.<sup>59</sup> Consequently, the tendency of the clusters to aggregate and finally merge would be restricted, so that nucleation becomes inhibited if it proceeds *via* cluster agglomeration. Such colloidal

stabilisation of  $\text{CaCO}_3$  prenucleation species against aggregation and nucleation has been reported also for other polymeric additives,<sup>40,41,43</sup> whereas changes in the structure of the clusters (possibly due to additive incorporation) were discussed as a reason for enhanced association in the presence of simple molecules like aspartic or citric acid.<sup>42,60,61</sup> Regardless of the particular mechanisms underlying the interactions between nucleating barium carbonate and added silica, the present results strongly suggest that the early stages of  $\text{BaCO}_3$  crystallisation may involve rather complex processes not envisaged by classical theories, which in many aspects appear to be similar to the comparatively well-studied  $\text{CaCO}_3$  case, but yet show certain important differences (*e.g.* lower stability of prenucleation clusters or the absence of a distinct amorphous intermediate phase).

In view of the formation of silica biomorphs, the most important effect identified in the titrations occurs in the early postnucleation stage, where the measured free ion products are dramatically higher in silica-containing solutions than in the reference experiment. In addition, the concentration of free ions does not reach a plateau over the studied period of time in most cases, but rather decreases monotonously (*cf.* Fig. 1). This shows that the high ion products observed after nucleation do not reflect the formation of a less stable and hence more soluble intermediate phase (stabilised by silica), for which a constant level of free ions in solution, dictated by the solubility product of the most soluble phase present, would be expected.<sup>47,52</sup> Nevertheless, the behaviour of the system can readily be understood when considering the structure and composition of the formed particles (*cf.* Fig. 3 and 4). In additive-free experiments, the  $\text{BaCO}_3$  crystals can grow freely and soon reach dimensions in the micron-range (*cf.* Fig. 3A–C); thus, the solid phase is in equilibrium with the surrounding solution (no growth inhibition), as is reflected in constant ion products after nucleation. In the presence of silica, the situation is drastically different; according to TEM and EDX analyses, the additive precipitates around the carbonate rods, thereby stabilising them at small particle sizes. Coating with silica impedes growth of  $\text{BaCO}_3$  and probably also delimits exchange of  $\text{Ba}^{2+}$  ions between the solid carbonate and the solution, both being essential for a constant solubility to be established. Furthermore, as growth cannot be simply continued, novel nucleation events will occur as the system is still far beyond saturation, leading to the formation of new nanoparticles that again will be embedded in silica. Therefore, supersaturation (*i.e.* the level of free  $\text{Ba}^{2+}$  and  $\text{CO}_3^{2-}$  in solution) can only gradually be diminished in a cascade of successive nucleation and – short – growth periods, which is fully in line with the slow decrease of the free ion product observed under these conditions.

Over time, this results in a multitude of uniform, silica-covered  $\text{BaCO}_3$  nanorods with sizes that are very close to those of the building blocks constituting silica biomorphs (typically 200–400 nm in length and up to 50 nm in width.<sup>16,17,20,21,24,27,45</sup> Interestingly, even the composition of the nanoparticles formed in the titration assays (Si/Ba atomic



ratio: 0.05–0.13, *cf.* Fig. S8 in the ESI†) is nearly identical to what has been reported for the nanocrystal units in the core of biomorphs (0.05–0.10).<sup>24</sup> This suggests that the effects identified in the present experiments are directly relevant for the formation of silica biomorphs; that is, the limitation of particle sizes to the nanoscale, as well as the concomitant high nucleation frequencies during self-assembly of the crystal aggregates, can be ascribed to the silicate species in solution. Indeed, similar conclusions were already drawn in previous studies by Aquilano and co-workers, who proposed that adsorption of silicate oligomers onto the surface of nucleating carbonate particles leads to a substantial decrease of interfacial tension and consequently to increased nucleation rates, which yield a large number of small particles.<sup>23,62</sup> Our results, however, do not support this notion (as we find that silica actually inhibits BaCO<sub>3</sub> nucleation) and rather indicate a scenario where miniaturisation of the building units is caused by the deposition of a continuous layer of amorphous silica around individual nanoparticles.

Precipitation of silica on the carbonate particles can be explained by local pH gradients that exist in the vicinity of carbonate surfaces growing in alkaline media, as proposed theoretically in recent studies<sup>20,21,26,27</sup> and confirmed experimentally by the data collected in the present work. Based on this model of coupled co-precipitation, it is furthermore possible to explain the distinct efficiency of silica to downsize the BaCO<sub>3</sub> crystals at different pH values. If this effect relies on a coating of the carbonate particles in a layer or matrix of silica, then the propensity of silica to condense and polymerise under the respective conditions should be a decisive factor. Correspondingly, the smallest crystallites (Fig. 3) and highest silica contents (Fig. S8 in the ESI†) were obtained at pH 10 and 600 ppm SiO<sub>2</sub>, where the oligomerisation tendency is the strongest.<sup>53,54</sup> While particles with somewhat larger sizes (yet in the nano-range) and lower Si counts were produced when increasing the pH to 10.5 and/or decreasing the silica concentration to 300 ppm, there is a marked and abrupt change in the behaviour at pH 11. Here, silica does not affect the crystal size to a large extent at 300 ppm, nor is it co-precipitated with the carbonate particles in any detectable amounts. This indicates that the mechanism of stabilisation cannot take place under these circumstances, which is reasonable in light of the concept of pH-based chemical coupling; on the one hand, the fraction of bicarbonate ions in equilibrium at pH 11 is rather low (~17%), so that the generation of a pH gradient due to local HCO<sub>3</sub><sup>-</sup> dissociation during BaCO<sub>3</sub> growth should be more difficult than at lower pH (at least any such gradient would be less pronounced). On the other hand, the solubility of silica is relatively high at pH 11,<sup>53</sup> and hence, the fewer protons released at the carbonate surface may not be sufficient to reach a critical level of supersaturation and trigger local silica precipitation. In turn, this seems to be possible when the silica concentration is raised to 600 ppm at pH 11, where – again – nanosized particles with significant amounts of associated silica were formed. These considerations further corroborate the idea of pH-induced

co-mineralisation of silica and carbonate at local length scales.

## Conclusions

In summary, our experiments have revealed detailed aspects of the nucleation and early growth stages of barium carbonate crystallisation in the presence of silica under conditions that reflect those typically applied for the preparation of self-assembled biomorphic materials. By a pH-constant titration methodology, we have observed that BaCO<sub>3</sub> precipitation is preceded by the formation of ion associates in solutions (ion pairs and/or clusters), and that nucleation occurs – in all likelihood – through aggregation and fusion of these precursors into spherical primary particles that then merge to yield rod-like nanocrystals (at least under the influence of silica).

The impact of silica as an additive during this process proved to be manifold and concerned virtually any of the investigated stages. First, we could identify a stabilising influence on BaCO<sub>3</sub> prenucleation species, presumably originating from binding of oligomeric silicates on solute clusters. Second, the initial nucleation step was progressively delayed, supposedly due to embedding and mutual shielding of small carbonate nuclei within a matrix of amorphous silica. Both of these effects were found to depend on the pH and the additive concentration in the samples, and could be correlated with the speciation of silica in solution under the respective conditions. Finally and most importantly, our data provide clear evidence that the presence of silica leads to a substantial miniaturisation of the resulting carbonate crystals, from rather ill-defined micron-sized rods to uniform elongated nanoparticles. This change can be ascribed to the deposition of extended silica layers around the evolving crystallites, which impedes further growth and ripening. The latter feature is also apparent in silica biomorphs, which are composed of exactly such sub-micron BaCO<sub>3</sub> crystallites as building blocks. While it has previously been conjectured that silica facilitates stabilisation of these nanometric units,<sup>20,21,26,27</sup> the present work provides direct proof for this claim and, moreover, confirms the notion that spontaneous precipitation of silica around the carbonate crystals results from local variations in pH. The observed stabilisation of prenucleation species and the simultaneous delay of nucleation may allow for high levels of supersaturation near the front of evolving biomorphs, which is an essential prerequisite for the envisaged autocatalytic mechanism of growth and would explain the large number of small crystallites produced in each of the consecutive nucleation events occurring during the development of these biomimetic crystal aggregates.<sup>26,27</sup>

All in all, the measurements performed in this study shed light on the nucleation of barium carbonate in general and, particularly, enable a much more profound understanding of the processes leading to the formation of well-defined building units in silica biomorphs, which may be translated to explore



the physical origin of other self-assembled hybrid materials as well.

## Acknowledgements

The authors thank Prof. Dr Helmut Cölfen (University of Konstanz) for support during the experiments and helpful discussions.

## Notes and references

- 1 T. Wang, J. Zhuang, J. Lynch, O. Chen, Z. Wang, X. Wang and D. LaMontagne, *Science*, 2012, **338**, 358–363.
- 2 C. A. Jones and M. R. Mirkin, *Nature*, 2012, **491**, 42–43.
- 3 M. Erb, R. Libanori, N. Rothfuchs and A. R. Studart, *Science*, 2012, **335**, 199–204.
- 4 J. Rieger, M. Kellermeier and L. Nicoleau, *Angew. Chem., Int. Ed.*, 2014, DOI: 10.1002/anie.201402890.
- 5 S.-H. Yu, H. Cölfen, K. Tauer and M. Antonietti, *Nat. Mater.*, 2005, **4**, 51–55.
- 6 T. Wang, A.-W. Xu and H. Cölfen, *Angew. Chem., Int. Ed.*, 2006, **45**, 4451–4455.
- 7 U. Tritschler, I. Zlotnikov, P. Zaslansky, P. Fratzl, H. Schlaad and H. Cölfen, *ACS Nano*, 2014, **8**, 5089–5104.
- 8 S.-H. Yu and H. Cölfen, *J. Mater. Chem.*, 2004, **14**, 2124–2147.
- 9 F. C. Meldrum and H. Cölfen, *Chem. Rev.*, 2008, **108**, 4332–4432.
- 10 L. B. Gower, *Chem. Rev.*, 2008, **108**, 4551–4627.
- 11 F. Nudelman and N. A. J. M. Sommerdijk, *Angew. Chem., Int. Ed.*, 2012, **51**, 6582–6596.
- 12 A. R. Studart, *Adv. Mater.*, 2012, **24**, 5024–5044.
- 13 F. Natalio, T. P. Corrales, M. Panthöfer, D. Schollmeyer, I. Lieberwirth, W. E. G. Müller, M. Kappl, H.-J. Butt and W. Tremel, *Science*, 2013, **339**, 1298–1302.
- 14 J. M. Garcia-Ruiz and J. L. Amoros, *J. Cryst. Growth*, 1981, **55**, 379–383.
- 15 J. M. Garcia-Ruiz, *J. Cryst. Growth*, 1985, **73**, 251–262.
- 16 J. M. Garcia-Ruiz, S. T. Hyde, A. M. Carnerup, A. G. Christy, M. J. Van Kranendonk and N. J. Welham, *Science*, 2003, **302**, 1194–1197.
- 17 S. T. Hyde, A. M. Carnerup, A.-K. Larsson, A. G. Christy and J. M. Garcia-Ruiz, *Physica A*, 2004, **339**, 24–33.
- 18 E. Bittarello and D. Aquilano, *Eur. J. Mineral.*, 2007, **19**, 345–351.
- 19 A. E. Voinescu, M. Kellermeier, B. Bartel, A. M. Carnerup, A.-K. Larsson, D. Touraud, W. Kunz, L. Kienle, A. Pfitzner and S. T. Hyde, *Cryst. Growth Des.*, 2008, **8**, 1515–1521.
- 20 J. M. Garcia-Ruiz, E. Melero-Garcia and S. T. Hyde, *Science*, 2009, **323**, 362–365.
- 21 W. Kunz and M. Kellermeier, *Science*, 2009, **323**, 344–345.
- 22 E. Melero-Garcia, R. Santisteban-Bailon and J. M. Garcia-Ruiz, *Cryst. Growth Des.*, 2009, **9**, 4730–4734.
- 23 E. Bittarello, F. R. Massaro and D. Aquilano, *J. Cryst. Growth*, 2010, **312**, 402–412.
- 24 M. Kellermeier, E. Melero-Garcia, F. Glaab, J. Eiblmeier, L. Kienle, R. Rachel, W. Kunz and J. M. Garcia-Ruiz, *Chem. – Eur. J.*, 2012, **18**, 2272–2282.
- 25 M. Kellermeier, J. Eiblmeier, E. Melero-Garcia, M. Pretzl, A. Fery and W. Kunz, *Cryst. Growth Des.*, 2012, **12**, 3647–3655.
- 26 M. Kellermeier, E. Melero-Garcia, W. Kunz and J. M. Garcia-Ruiz, *J. Colloid Interface Sci.*, 2012, **380**, 1–7.
- 27 M. Kellermeier, H. Cölfen and J. M. Garcia-Ruiz, *Eur. J. Inorg. Chem.*, 2012, **32**, 5123–5144.
- 28 J. Eiblmeier, M. Kellermeier, D. Rengstl, J. M. Garcia-Ruiz and W. Kunz, *CrystEngComm*, 2013, **15**, 43–53.
- 29 W. L. Noorduin, A. Grinthal, L. Mahadevan and J. Aizenberg, *Science*, 2013, **340**, 832–837.
- 30 M. Kellermeier, F. Glaab, E. Melero-Garcia and J. M. Garcia-Ruiz, *Methods Enzymol.*, 2013, **532**, 225–256.
- 31 G. Zhang, J. M. Delgado-Lopez, D. Choquesillo-Lazarte and J. M. Garcia-Ruiz, *CrystEngComm*, 2013, **15**, 6526–6532.
- 32 J. M. Garcia-Ruiz, *Geology*, 1998, **26**, 843–846.
- 33 J. M. Garcia-Ruiz, A. Carnerup, A. G. Christy, N. J. Welham and S. T. Hyde, *Astrobiology*, 2002, **2**, 353–369.
- 34 M. Kellermeier, E. Melero-Garcia, F. Glaab, R. Klein, M. Drechsler, R. Rachel, J. M. Garcia-Ruiz and W. Kunz, *J. Am. Chem. Soc.*, 2010, **132**, 17859–17866.
- 35 J. Eiblmeier, M. Kellermeier, M. Deng, L. Kienle, J. M. Garcia-Ruiz and W. Kunz, *Chem. Mater.*, 2013, **25**, 1842–1851.
- 36 D. Gebauer, A. Völkel and H. Cölfen, *Science*, 2008, **322**, 1819–1822.
- 37 M. Kellermeier, H. Cölfen and D. Gebauer, *Methods Enzymol.*, 2013, **532**, 45–69.
- 38 M. Kellermeier, A. Picker, A. Kempster, H. Cölfen and D. Gebauer, *Adv. Mater.*, 2014, **26**, 752–757.
- 39 W. E. J. M. Habraken, J. Tao, L. J. Brylka, H. Friedrich, L. Bertinetti, A. S. Schenk, A. Verch, V. Dmitrovic, P. H. H. Bomans, J. Laven, P. Van Der Schoot, B. Aichmayer, G. De With, J. J. De Yoreo and N. A. J. M. Sommerdijk, *Nat. Commun.*, 2013, **4**, 1507.
- 40 D. Gebauer, H. Cölfen, A. Verch and M. Antonietti, *Adv. Mater.*, 2009, **21**, 435–439.
- 41 A. Verch, D. Gebauer, M. Antonietti and H. Cölfen, *Phys. Chem. Chem. Phys.*, 2011, **13**, 16811–16820.
- 42 A. Picker, M. Kellermeier, J. Seto, D. Gebauer and H. Cölfen, *Z. Kristallogr.*, 2012, **227**, 744–757.
- 43 A. Rao, J. K. Berg, M. Kellermeier and D. Gebauer, *Eur. J. Mineral.*, 2014, **26**, 537–552.
- 44 A. E. Voinescu, M. Kellermeier, A. M. Carnerup, A.-K. Larsson, D. Touraud, S. T. Hyde and W. Kunz, *J. Cryst. Growth*, 2007, **306**, 152–158.
- 45 M. Kellermeier, F. Glaab, A. M. Carnerup, M. Drechsler, B. Gossler, S. T. Hyde and W. Kunz, *J. Cryst. Growth*, 2009, **311**, 2530–2541.
- 46 D. G. Hall, *J. Phys. Chem.*, 1996, **100**, 7230–7236.



- 47 D. Gebauer and H. Cölfen, *Nano Today*, 2011, **6**, 564–584.
- 48 P.-C. Cheng, G. Y. Cheng, M. H. Kou, P. Y. Shia and P. O. Chung, *J. Cryst. Growth*, 2001, **226**, 458–472.
- 49 P. Raiteri and J. D. Gale, *J. Am. Chem. Soc.*, 2010, **132**, 17623–17634.
- 50 T. Z. Forbes, A. V. Radha and A. Navrotsky, *Geochim. Cosmochim. Acta*, 2011, **75**, 7893–7905.
- 51 A. E. S. Van Driessche, L. G. Benning, J. D. Rodriguez-Blanco, M. Ossorio, P. Bots and J. M. Garcia-Ruiz, *Science*, 2012, **336**, 69–72.
- 52 D. Gebauer, M. Kellermeier, J. D. Gale, L. Bergström and H. Cölfen, *Chem. Soc. Rev.*, 2014, **43**, 2348–2371.
- 53 R. K. Iler, *The chemistry of silica. Solubility, polymerization, colloid and surface properties, and biochemistry*, John Wiley & Sons, New York, 1979.
- 54 S. Sjöberg, *J. Non-Cryst. Solids*, 1996, **196**, 51–57.
- 55 L. Svensson and L. O. Öhman, *J. Chem. Soc., Faraday Trans.*, 1986, **82**, 3635–3646.
- 56 W. L. Marshall and J. M. Warakomski, *Geochim. Cosmochim. Acta*, 1980, **44**, 915–924.
- 57 J. P. R. de Villiers, *Am. Mineral.*, 1971, **56**, 758–766.
- 58 E. M. Pouget, P. H. H. Bomans, J. A. C. M. Goos, P. M. Frederik, G. De With and N. A. J. M. Sommerkijk, *Science*, 2009, **323**, 1455–1458.
- 59 M. Kellermeier, D. Gebauer, E. Melero-Garcia, M. Drechsler, Y. Talmon, L. Kienle, H. Cölfen, J. M. Garcia-Ruiz and W. Kunz, *Adv. Funct. Mater.*, 2012, **22**, 4301–4311.
- 60 A. R. Finney and P. M. Rodger, *Faraday Discuss.*, 2012, **159**, 47–60.
- 61 P. Raiteri, R. Demichelis, J. D. Gale, M. Kellermeier, D. Gebauer, D. Quigley, L. B. Wright and T. R. Walsh, *Faraday Discuss.*, 2012, **159**, 61–85.
- 62 E. Bittarello, F. R. Massaro, M. Rubbo, E. Costa and D. Aquilano, *Cryst. Growth Des.*, 2009, **9**, 971–977.

